

Uniformizing Lee-Yang Singularities

Gökçe Başar^{*1}, Gerald V. Dunne^{†2}, and Zelong Yin^{‡1}

¹Department of Physics and Astronomy, University of North Carolina, Chapel Hill, NC 27599

²Physics Department, University of Connecticut, Storrs, CT 06269-3046

Abstract

Motivated by the search for the QCD critical point, we discuss how to obtain the singular behavior of a thermodynamic system near a critical point, namely the Lee-Yang singularities, from a limited amount of local data generated in a different region of the phase diagram. We show that by using a limited number of Taylor series coefficients, it is possible to reconstruct the equation of state past the radius of convergence, in particular in the critical region. Furthermore we also show that it is possible to extend this reconstruction to go from a crossover region to the first-order transition region in the phase diagram, using a uniformizing map to pass between Riemann sheets. We illustrate these ideas via the Chiral Random Matrix Model and the Ising Model.

1 Introduction

Mapping the phase structure of QCD plays an important role in understanding the structure of matter in extreme environments, both theoretically and experimentally. A particularly important aspect of this endeavor is the ongoing search for the QCD critical point, a singular point in the phase diagram where a smooth crossover between the hadronic phase and the quark-gluon plasma phase turns into a first-order transition. It is one of the major motivations of the Beam Energy Scan program at the Relativistic Heavy-Ion Collider as well as future heavy-ion facilities [1]. Quantitative theoretical knowledge of the QCD critical point and the equation of state in its vicinity is crucial for the experiments to identify critical point signatures [2].

The fermion sign problem complicates the use of lattice QCD to explore the phase diagram at non-zero baryon chemical potential, μ_B , where the critical point is conjectured to exist. Without direct access to the phase diagram, typical methods to extract information on the phase diagram at finite density include Taylor expanding around $\mu_B = 0$ [3], simulating QCD with an imaginary chemical potential where there is no sign problem and analytically continuing to real values [4], and resummation methods some of which incorporate both [5, 6, 7, 8, 9].

At the same time, even without a direct calculation of the critical point it is still possible to predict some of its properties, if it exists. This is due to the fact that based on general symmetry arguments, the QCD critical point is in the same static universality class as the three dimensional Ising model [10]. Universality essentially relates the singular contribution to the QCD equation of state to the equation of state of the Ising model in the vicinity of the critical point. This fixes the critical exponents which determine how certain thermodynamic functions diverge. However, the precise form of this relation is not determined by universality. The relationship between the Ising parameters (namely the reduced temperature r and the magnetic field h) and those of QCD (the temperature T and chemical potential μ) is not determined by universality and has to be extracted directly from QCD [2]. Likewise, the location of the critical point is also a non-universal quantity.

*gbasar@unc.edu

†gerald.dunne@uconn.edu

‡zelong@live.unc.edu

In this paper we tackle these issues from the perspective of series expansions: given a finite-order series expansion around $\mu = 0$, we describe improved methods for extracting physical information regarding the singularities of the equation of state in the vicinity of the critical point. In particular we show that with a suitably chosen resummation scheme it is possible to: i) extract the location of the nearest complex singularities, the Lee-Yang edge singularities, which can be used to determine the location of the critical point and constrain the singular contribution to the equation of state; and ii) analytically continue the equation of state across different Riemann sheets in a way that relates the high temperature crossover region to the low temperature first-order transition region. These ideas follow closely Ref. [11], whose mathematical foundations can be found in Refs. [12, 13].

The paper is organized as follows. In Section 2 we briefly summarize the relevant properties of the Chiral Random Matrix Model model that we use to motivate and illustrate our framework. In Section 3 we explain how to construct the Lee-Yang edge singularities from a series expansion by using the conformal-Padé method, and further to extract the critical point and constrain the equation of state. In Section 4 we focus on a different problem and explain how the equation of state can be analytically continued across different Riemann sheets using a different resummation scheme which we call “uniformized-Padé”. In the conclusions we briefly discuss the outlook for future extensions.

2 The chiral random matrix model

We introduce the ideas that we develop in this paper via the Chiral Random Matrix Model [14], which shares some of the key properties with the conjectured QCD phase diagram, such as chiral symmetry breaking and chiral restoration at large chemical potential, as well as the existence of a critical point along this transition curve. In this section we review some of its known properties that will be relevant in our analysis. Readers who are familiar with the model can skip this section.

The Chiral Random Matrix Model is a toy model for QCD where the matrix elements of the Dirac matrix are replaced by Gaussian random variables. Its partition function for N_f number of fermions is

$$Z(T, \mu) = \int \mathcal{D}\Phi e^{-N\text{Tr}(\Phi\Phi^\dagger)} \prod_{f=1}^{N_f} \det^{N/2} \begin{pmatrix} \Phi + m_f & \mu + iT \\ \mu + iT & \Phi^\dagger + m_f \end{pmatrix} \det^{N/2} \begin{pmatrix} \Phi + m_f & \mu - iT \\ \mu - iT & \Phi^\dagger + m_f \end{pmatrix} \quad (1)$$

where the integration is over all $N \times N$ complex matrices Φ . We work with $N_f = 1$ for the rest of the paper and denote the quark mass as m_q . In the $N \rightarrow \infty$ limit the path integral is saturated by the saddle point where the matrix Φ is proportional to the unit matrix, $\Phi = \phi \times \mathbb{1}_{N \times N}$ with $\phi \in \mathbb{R}$:

$$\lim_{N \rightarrow \infty} \frac{1}{N} \log Z(T, \mu) = - \min_{\phi} \Omega(T, \mu, \phi) \quad (2)$$

$$\Omega(T, \mu, \phi) = \phi^2 - \frac{1}{2} \log [((\phi + m_q)^2 - (\mu + iT)^2) ((\phi + m_q)^2 - (\mu - iT)^2)] . \quad (3)$$

As usual the minimization of the free energy determines the equation of state where the pressure is identified as $p(T, \mu) = - \min_{\phi} \Omega(T, \mu, \phi)$. The phase diagram of this Chiral Random Matrix Model is shown in Fig. 1. For $m_q = 0$ and small values of T and μ , the ground state is given by $\phi \neq 0$, which breaks chiral symmetry. At larger values of T and/or μ , chiral symmetry is restored via a second or first order transition, as shown in the figure as blue and red lines respectively. For a fixed $m_q > 0$, the chiral symmetry is explicitly broken but the remnant of the second order transition still persists as a rapid crossover. For lower temperatures this crossover turns into a first order transition (red lines in the figure). The point where the crossover turns into a first order transition is a second order critical point. As a function of m_q the critical point follows a trajectory in the three dimensional T, μ, m_q space, as shown in Figure 1.

We are specifically interested in the physics near the critical point where

$$\frac{\partial}{\partial \phi} \Omega(T, \mu, \phi) = \frac{\partial^2}{\partial \phi^2} \Omega(T, \mu, \phi) = 0. \quad (4)$$

Let us denote the point where a real solution exists as $T = T_c, \mu = \mu_c$, and $\phi = \phi_c$.¹ The susceptibility and

¹As we will explain further, as a particular property of the mean field limit, T_c corresponds to the largest temperature such a solution exists.

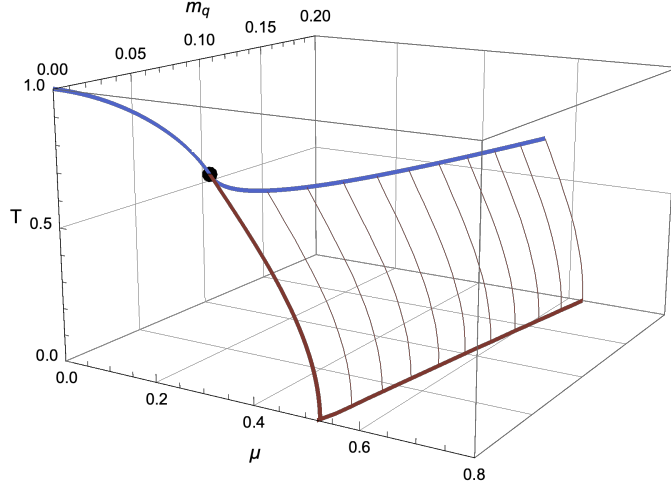


Figure 1: The phase diagram of the Chiral Random Matrix Model. Red and blue curves represent the first and second-order transitions and the black dot represents the tri-critical point where the first and second order transitions meet at $m_q=0$. For nonzero values of m_q the tri-critical point turns into a second order critical point with mean field exponents parameterized by m_q , $(T_c(m_q), \mu_c(m_q))$.

the heat capacity diverge as power laws at the critical point. Furthermore, the singular part of the equation of state in the vicinity of the critical point is essentially the same as that of the Ising model in the mean field limit, since the Chiral Random Matrix Model and the Ising model are in the same static universality class. The same holds for QCD as well, but in this case it is the three dimensional Ising model as opposed to the Ising model in the mean field limit.

In the continuum limit and d -dimensions, the Ising model is described by a scalar field with the action

$$S = \int d^d x \left[\frac{1}{2}(\partial_\mu \phi)^2 + \frac{1}{2}r_0 \phi^2 + \frac{1}{4}u_0 \phi^4 \right] \quad (5)$$

In $d \leq 4$ dimensions r_0 and u_0 flow to the Gaussian fixed point where u_0 becomes arbitrarily small and the theory can be described by mean field theory. In mean field theory, the equation of state follows from minimizing the effective potential

$$\Omega_I(M) = -hM + \frac{1}{2}rM^2 + \frac{1}{4}M^4 \quad (6)$$

where M is the average magnetization $M = \langle \phi \rangle$. For convenience we have re-scaled ϕ to set the coefficient of the quartic term to $1/4$. The equation of state is obtained by minimizing the effective potential:

$$\frac{\partial \Omega_I(M)}{\partial M} = -h + rM + M^3 = 0. \quad (7)$$

The critical point is located at $\partial \Omega_I(M)/\partial M = \partial^2 \Omega_I(M)/\partial M^2 = 0$, which corresponds to $r = h = 0$. For fixed $r > 0$, the magnetization smoothly crosses over from $M < 0$ to $M > 0$ as the magnetic field varies from $h < 0$ to $h > 0$. For $r < 0$ this transition is first order. As is typical in first order transitions for $r < 0$ and $h < 0$, in addition to the global minimum state with $M < 0$ there is also a meta-stable state with $M > 0$. The point in the phase diagram (for fixed r) where the meta-stable state ceases to exist is the spinodal point. The equation of state (7) is invariant under scaling $r \rightarrow \lambda r$, $h \rightarrow \lambda^{3/2} h$, $M \rightarrow \lambda^{1/2} M$. Therefore it is convenient to express the minimization in terms of the scaling variables, $w := hr^{-3/2}$ and $z := Mr^{-1/2}$, as:

$$w = z + z^3. \quad (8)$$

In the vicinity of the critical point, the equation of state of the Chiral Random Matrix model can be mapped to that of the Ising model. Let us first expand the temperature and the chemical potential around

the critical point as $\Delta T = T - T_c$, $\Delta\mu = \mu - \mu_c$. They can be mapped into the the Ising variables r and h linearly as

$$h = h_T \Delta T + h_\mu \Delta\mu, \quad r = r_T \Delta T + r_\mu \Delta\mu \quad (9)$$

To see how this mapping works let us follow the steps in [15] and expand $\Omega(\phi)$ around the critical point

$$\Omega(\phi) = \Omega(\phi_c) + f_1(T, \mu)\delta\phi + f_2(T, \mu)\delta\phi^2 + \dots \quad (10)$$

where $\delta\phi = \phi - \phi_c$. Further expanding f_i around T_c, μ_c and eliminating the $\delta\phi^3$ term via shifting $\delta\phi$ by a constant we have

$$\Omega(\phi) = \Omega_0 - \bar{h}\delta\phi + \frac{\bar{r}}{2}\delta\phi^2 + \frac{u}{4}\delta\phi^4 + vu\delta\phi^5 + \mathcal{O}(\delta\phi^6) \quad (11)$$

where the $\delta\phi^5$ term is necessary to take into account the correction to scaling that is present in Eq. (9) since h and r have scale differently ($h \sim r^{3/2}$). This quintic term can be eliminated via $\delta\phi \rightarrow \delta\phi + v(\bar{r}/u - \delta\phi^2)$ to leading order in r . Finally rescaling the field so that the coefficient of the quadratic term is 1/4 leads to the Ising form

$$\Omega(\phi) = \Omega_0 - h\delta\phi + \frac{r}{2}\delta\phi^2 + \frac{1}{4}\delta\phi^4 + \dots \quad (12)$$

Here $h = u^{-1/4}\bar{h}$, and $r = u^{-1/2}(\bar{r} + 2v\bar{h})$ in leading order in \bar{r} . Since \bar{r} and \bar{h} are obtained from expanding f_1 and f_2 to linear order in ΔT and $\Delta\mu$, from these expressions we can read off the mapping parameters (h_T, h_μ, r_T, r_μ) . For example, for $m_q = 0.1$ we obtain $(h_\mu, h_T, r_\mu, r_T) \approx (-1.692, -0.452, 0.315, 2.481)$ with $\tan \alpha_1 \equiv h_\mu/h_T \approx 3.739$ and $\tan \alpha_2 \equiv r_\mu/r_T \approx 0.127$ (see Fig. 2).

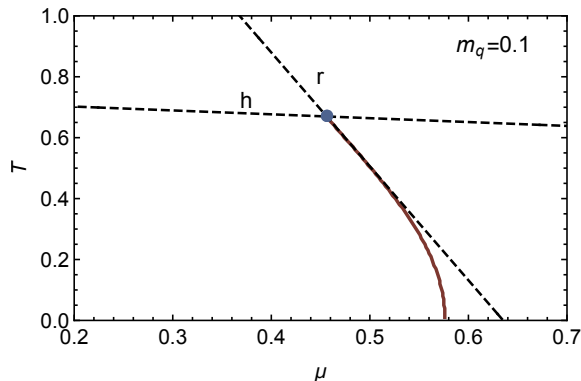


Figure 2: The Ising model parameters mapped to the (T, μ) plane of the chiral random matrix model. The slopes of the r and h axes are $\tan \alpha_1 \equiv h_\mu/h_T$ and $\tan \alpha_2 \equiv r_\mu/r_T$, respectively. For $m_q = 0.1$ the critical point is at $T_c \approx 0.67$ and $\mu_c \approx 0.46$.

2.1 Lee-Yang edge singularities

For $m_q > 0$, the critical point (4) is a singular point in the phase diagram. However, in general, for $T \neq T_c$ this condition is satisfied for a pair of complex conjugate values μ . These points correspond to the celebrated Lee-Yang (LY) edge singularities [16] which will denote as $\mu_{LY}(T)$. As T approaches T_c from above they pinch the real axis such that $\mu_{LY}(T_c) = \mu_c$.

More generally, the finite N partition function, (1) is a polynomial in μ of order $2N \times N_f$, which therefore has $2N \times N_f$ zeros. As $N \rightarrow \infty$ they form branch cuts and $\mu_{LY}(T)$ are the branch points associated with these cuts [17, 18].

In the context of the critical point, we would like to analyze $\mu_{LY}(T)$ in the vicinity of the critical point. Using universality, we can turn to the Ising model where the Lee-Yang singularity is simply $dw/dz = 0$,

which from Eq. (8) leads to $w_{LY} = \pm i2/(3\sqrt{3})$.² The LY singularity can be viewed as a critical point and in its vicinity the equation of state behaves as

$$z - z_{LY} \propto (w - w_{LY})^{\sigma_{LY}} \quad (13)$$

where $\sigma_{LY} = 1/2$ is the associated critical exponent. Beyond the mean field limit, the critical equation of state in the vicinity of the LY singularity is described by the ϕ^3 theory with pure imaginary coupling [20] with $\sigma \approx 0.074 - 0.085$. Using the mapping back to the random matrix model, Eq. (9), we obtain

$$\mu_{LY}(T) \approx \mu_c + K_1(T - T_c) \pm iK_2(T - T_c)^{3/2} \quad \text{where} \quad K_1 = -\frac{h_T}{h_\mu}, \quad K_2 = \frac{2}{3\sqrt{3}} \frac{r_\mu^{3/2}}{h_\mu} \left(\frac{r_T}{r_\mu} - \frac{h_T}{h_\mu} \right)^{3/2}. \quad (14)$$

It is worth noting that $\mu_{LY}(T)$ is real for $T < T_c$. In this regime they correspond to the location of the spinodal point. The fact that they lie on the real axis for $T < T_c$ is an artifact of the mean field limit. In general, the sub-leading term in Eq. (14) is proportional to $(T - T_c)^{\beta\delta}$ where β and δ are the usual critical exponents. In mean field theory $\beta\delta = 3/2$ and the sub-leading term becomes real for $T < T_c$. Beyond mean field this is not the case, which has interesting consequences for the spinodal singularities [21, 22, 23].

The LY trajectory given in Eq. (14) is the main starting point of our analysis. Our strategy in the next section will be to reconstruct this expansion near T_c from a truncated series expansion of the equation of state. Then one can obtain the location of T_c , μ_c , as well as K_1 and K_2 which contain the mapping parameters to the Ising model. More generally, the LY singularities in the context of QCD critical point have been discussed in, for example, [24, 25, 18, 26, 19, 27, 28].

3 The conformal map and the Lee-Yang trajectory

In this section we explain how to determine the location of the LY singularities with high precision in the practical situation where we only have access to approximate information about the equation of state. Furthermore, this approximate information is typically computed in a region away from the critical region, and yet we are most interested in probing the vicinity of the critical point (see for example [29]). Due to the fermion sign problem, most commonly the region we have access to is around $\mu = 0$ (see [4] for a recent review), and the information we have is typically a local Taylor expansion around this point. For concreteness let us focus on the susceptibility,

$$\chi(T, \mu) = \frac{\partial^2 p(T, \mu)}{\partial \mu^2} \approx \sum_{n=0}^N c_n(T) \mu^{2n}. \quad (15)$$

The natural expansion parameter is μ^2 , similar to QCD in which case is due to the charge conjugation symmetry. Even though this is a *local* expansion around $\mu = 0$, it contains *global* information, including especially the singular behavior around $\mu = \mu_{LY}$. This information is encoded in the coefficients $c_n(T)$, and our task is to decode it as efficiently and precisely as possible. Optimizing this decoding procedure is important as in many cases we only have access to the first few terms in the local expansion. In this section we introduce an efficient framework that not improves the approximation to the LY singularity compared to other methods, but also provides an accurate approximation to the equation of state in the critical region. The ideas we pursue here are built upon techniques developed in [12, 13], and which have recently been applied to the Gross-Neveu model in Ref. [11]. Here we apply them to the Random Matrix Model and detail the technical aspects of the framework.

In general since $\mu^2 = \mu_{LY}^2$ is the closest singularity to the origin, the radius of convergence of the Taylor expansion in Eq. 15 is $|\mu_{LY}^2|$. However the coefficients $c_n(T)$ contain much more information than just the radius of convergence. The Darboux theorem [30, 29] states that the behavior of the coefficients $c_n(T)$ at large order n is directly related to the behavior of the function in the vicinity of the nearest singularity. Specifically, if the Taylor expansion coefficients of a function $f(z) = \sum_{n=0}^{\infty} b_n z^n$ near the origin have leading large-order growth as $n \rightarrow \infty$:

$$b_n \sim \frac{1}{z_0^n} \left[\binom{n+g-1}{n} \phi(z_0) - \binom{n+g-2}{n} z_0 \phi'(z_0) + \binom{n+g-3}{n} \frac{z_0^2}{2!} \phi''(z_0) - \dots \right] \quad (16)$$

²Beyond the mean field limit this value has been computed in Ref. [19] for the three dimensional $O(N)$ symmetric model.

then the leading singularity is located at z_0 , and in the vicinity of z_0 the function behaves as

$$f(z) \sim \phi(z) \left(1 - \frac{z}{z_0}\right)^{-g} + \psi(z) \quad , \quad z \rightarrow z_0 \quad (17)$$

where $\phi(z)$ and $\psi(z)$ are analytic near z_0 . This means that from a detailed study of the expansion coefficients $c_n(T)$, derived from the expansion about $\mu = 0$, we can learn about the expansion of the function near the critical point. The leading term in (16) tells us the location of the singularity, as well as its exponent g and its strength $\phi(z_0)$. The further subleading terms contain information about the expansion of $\phi(z)$ in the vicinity of the critical point. The practical question is: what is the most efficient way to extract as much of this information as possible, from a limited number of $c_n(T)$ coefficients? Optimized strategies for this problem have been developed recently in [12, 13].

3.1 The Padé Approximant and the Radius of Convergence

Away from T_c , the Lee-Yang singularities occur as a complex conjugate pair. Since they are equidistant from the origin they both contribute, with equal weight but with phase of opposite sign. Hence the large-order growth of the expansion coefficients $c_n(T)$ exhibits oscillatory behavior at large order, due to interference between the complex conjugate pair of LY singularities.

$$c_n(T) \sim |\chi(\mu_{LY}(T))| \binom{n - \sigma_{LY} - 1}{n} \frac{\cos(n\theta_{LY}(T) + \delta_{LY}(T))}{|\mu_{LY}^2(T)|^n} \quad , \quad n \rightarrow \infty \quad (18)$$

where $\theta_{LY} = \arg \mu_{LY}^2$, and δ_{LY} is the phase offset. The parameter σ_{LY} determines the nature of the singularity. This oscillatory behavior makes it numerically challenging to extract the relevant physical quantities (such as the location of μ_{LY} , and the critical exponent, σ_{LY}) directly from ratio tests or root tests of the coefficients $c_n(T)$. See Figure 3, in which we show the large order behavior of the ratio tests and the root tests of the coefficients, and compare with the exact radius of convergence for a fixed value temperature, $T \approx 1.34T_c$. The interference effect is highly pronounced in the ratios which makes the extraction of $|\mu_{LY}^2|$ difficult. The root test provides better convergence as the oscillating envelope is damped. However one still needs a large number of terms until this damping occurs. An alternative and significantly more efficient way to extract the singular behavior of the equation of state is to use Padé approximants. Figure 3 shows significantly faster convergence for extracting the radius of convergence.

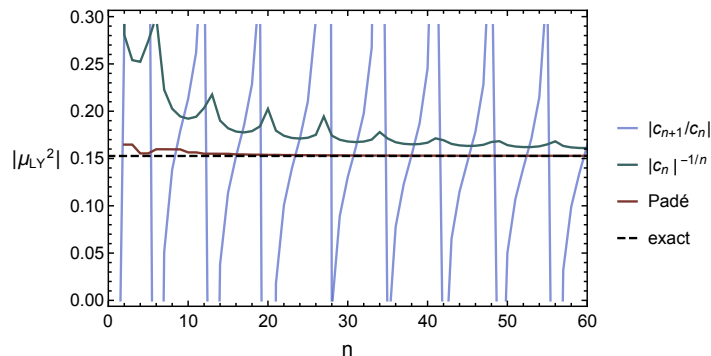


Figure 3: The distance from the LY singularity to the origin, $|\mu_{LY}^2|$, extracted from a fixed number n of coefficients $c_n(T)$ of the Taylor series expansion of the equation of state Eq. (15), using different methods. Here $m_q = 0.1$ and $T = 0.9$. The dashed horizontal line is the exact value at this temperature. The simple ratio test $|c_{n+1}(T)/c_n(T)|$ shows wild oscillations about the exact value, while the root test $|c_n(T)|^{1/n}$ is better behaved but converges slowly. Padé methods are much more accurate with many fewer terms.

Padé methods provide an excellent, and simple, low-resolution probe of the singularity structure, and this can then be further refined by combining with conformal and uniformizing maps, as described below.

The idea is to approximate the original function by a rational function [31, 32],

$$P[\chi(T, \mu)] = \frac{k_0(T) + k_1(T)\mu^2 + \dots + k_{N/2}(T)\mu^N}{l_0(T) + l_1(T)\mu^2 + \dots + l_{N/2}(T)\mu^N}. \quad (19)$$

where we consider N to be even. Here the coefficients k_i and l_i are determined by expanding Eq. (19) in μ^2 and matching with the original expansion, Eq. (15). This procedure is completely algorithmic, and is a built-in operation in symbolic software such as Mathematica and Maple. It is worth noting that the label T in Eq. (19) should be viewed as an index rather than an argument of a smooth function, because the Padé polynomials do not necessarily change smoothly when the coefficients $c_n(T)$ change smoothly. In general the order of the polynomials in the denominator and numerator could be different as long as there are $N + 1$ independent coefficients. Here we consider the diagonal case where they have the same order unless specified otherwise, but it is important to note that numerical stability can be probed by varying the degrees of the Padé polynomials.

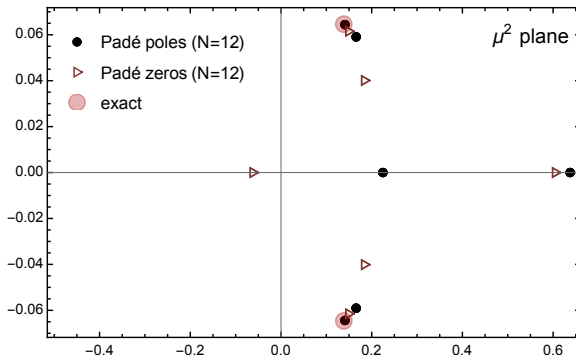


Figure 4: The poles and zeros of Padé approximants with 12 terms for $m_q = 0.1$ and $T = 0.9 \approx 1.34T_c$. Note the different scales on the two axes: the argument θ_{LY} of μ_{LY}^2 is quite small. In representing a complex conjugate pair of branch points, Padé constructs a curved arc of poles and zeros joining the two branch points, together with another line of poles and zeros emanating from the first arc and extending to infinity along the real axis. This latter line is an artifact of Padé, not a feature of the underlying function [33, 34, 13].

In contrast with the truncated Taylor expansion (15), the corresponding Padé approximant has poles. Along with the zeros they approximate the location of the leading singularity. For a function with branch points, Padé represents the branch points as the accumulation points (in the $N \rightarrow \infty$ limit) of arcs of interlacing poles and zeros, whose shape is determined by minimizing an effective electrostatic capacitance [33, 34, 12, 13]. We see in Figure 4 that even with relatively few coefficients ($N = 12$), the branch point locations in the complex plane can be estimated very accurately. Below we describe an iterative method to refine this initial estimate to even higher precision. See Fig. 8. Figure 3 shows the value of $|\mu_{LY}^2|$ extracted from Padé resummation, plotted as a function of the number of input coefficients. We chose the pole that is closest to origin and in order to eliminate some of the unphysical singularities filtered out those with residues smaller than 10^{-6} . The results are stable under variations of the cutoff and the Padé orders. In Figure 3 we see that the convergence to the exact result is much faster and more accurate than either the ratio or root tests. Furthermore, Figure 4 shows that the Padé approximant gives direct access to the full complex form of μ_{LY}^2 , not just the magnitude $|\mu_{LY}^2|$. It is also important to note that this result is obtained by using the *same input* as the truncated Taylor expansion, namely just the series coefficients, without any additional input.

In addition to providing a significantly better way of locating its singularities, Padé approximants can also be used to improve the accuracy of the approximation to the equation of state and the susceptibilities. In Fig. 7 we show the result of the Padé approximant for the susceptibility, as well as for the higher order susceptibilities

$$\chi_n(T, \mu) = \frac{\partial^n p(T, \mu)}{\partial \mu^n} \quad (20)$$

These observables, especially χ_3 and χ_4 , play a crucial role in the search for the critical point as their magnitude grows in the vicinity of the critical point. Their counterparts in QCD are related to the skewness and kurtosis of the net baryon number distribution [2]. Furthermore, their shape and quantitative features depend non-trivially on the mapping parameters given in Eq. (9) [15]. Therefore it is vitally important to obtain an accurate approximation to the equation of state in order to resolve this structure. As seen in Fig. 7, the Padé approximant slightly outperforms the truncated Taylor series, which diverges at $\mu^2 = |\mu_{LY}^2|$ as expected. However, Padé also diverges for $\mu^2 \gtrsim |\mu_{LY}^2|$. This is because it hits an unphysical pole along the real axis.

The existence of these unphysical poles, as highlighted in Fig. 4, is an inherent shortcoming of Padé when there is a complex conjugate pair of branch points. For such a configuration, in minimizing the effective capacitance, Padé places spurious unphysical poles and zeros along the positive real axis, extending out to infinity and becoming dense as $N \rightarrow \infty$ [33, 34, 12, 13].³ The effect of these spurious poles and zeros can be seen in Fig. 7, where they are responsible for the large unphysical oscillations of the Padé-reconstructed susceptibilities beyond the radius of convergence. This unphysical effect can be overcome by using conformal or uniformizing maps in conjunction with Padé, as described below, thereby significantly extending the range of applicability of the resummation.

3.2 The Conformal Padé Method

Up to this point we have not used any additional information other than the expansion coefficients. We could further improve the accuracy of our approximation by providing more information. For example, we know that for $T > T_c$, the equation of state has two complex conjugate branch points, $|\mu_{LY}^2|e^{\pm i\theta}$ [18, 22] as well as a critical exponent, even beyond the mean field limit. We can incorporate this information before making the Padé approximation.

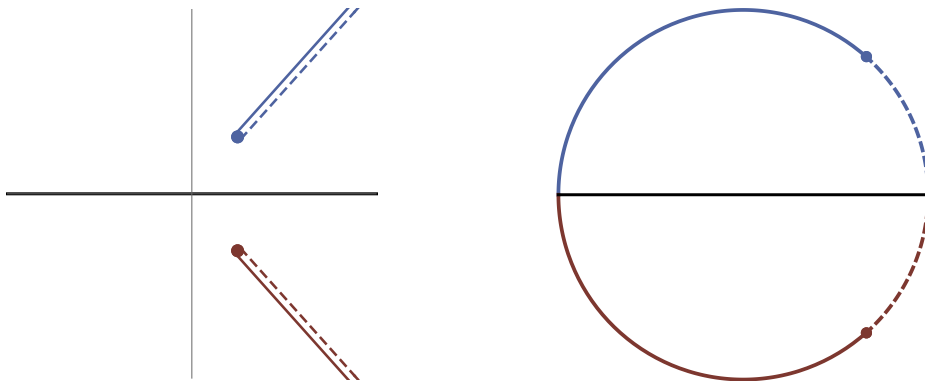


Figure 5: The singularity structure in the μ^2 plane for $T > T_c$ where the dots denote the LY singularities and the lines denote symmetrically chosen branch cuts (left) and its image on the unit disk under the conformal map Eq. (21) (right).

The first step is to conformally map the μ^2 plane into the unit disk ($|\zeta| < 1$) by identifying μ^2 with $\phi(\zeta)$. Conformal maps have well known applications in summation methods [35, 36, 37, 13]. Here we need a conformal map for a complex conjugate pair of singularities, as shown in Figure 5 [left]. We use the conformal map, $\phi(\zeta)$, where

$$\phi(\zeta) = 4|\mu_{LY}^2| \left(\frac{\theta}{\pi}\right)^{\theta/\pi} \left(\frac{1-\theta}{\pi}\right)^{1-\theta/\pi} \frac{\zeta}{(1+\zeta)^2} \left(\frac{1+\zeta}{1-\zeta}\right)^{2\theta/\pi} \quad (21)$$

This maps the μ^2 plane into the unit disk as shown in Fig. 5.⁴ The branch points (the LY singularities) and the associated cuts (red, blue dots and lines) are mapped onto the boundary of the unit disk. Notice that

³These spurious poles and zeros are distinct from other spurious poles and zeros due to numerical instabilities from lack of precision.

⁴See [38, 39]. This particular map appears in a wide range of physical applications [40, 41, 42].

each side of each cut (depicted as a dashed or solid line) is mapped to a different segment of the unit circle, meeting at the associated branch point and at $\zeta = \pm 1$, corresponding to the point at infinity.

The next step is to re-expand the susceptibility $\chi(T, \phi(\zeta))$ as a series in ζ instead of as a series in μ^2 , truncating at the same order (this procedure is optimal [12]):

$$\chi(T, \phi(\zeta)) \approx \sum_{n=0}^N \tilde{c}_n(T) \zeta^n \quad (22)$$

followed by a Padé approximant (now in terms of ζ) of this re-expansion. Let us denote the poles and zeros of this modified Padé approximant as ζ_i for $i = 1, \dots, N$. Using the conformal map (21) we map them back to the μ^2 plane:

$$\mu_i^2 = \phi(\zeta_i). \quad (23)$$

Similar to Padé singularities, the μ_i^2 values accumulate towards the physical singularities, μ_{LY}^2 .

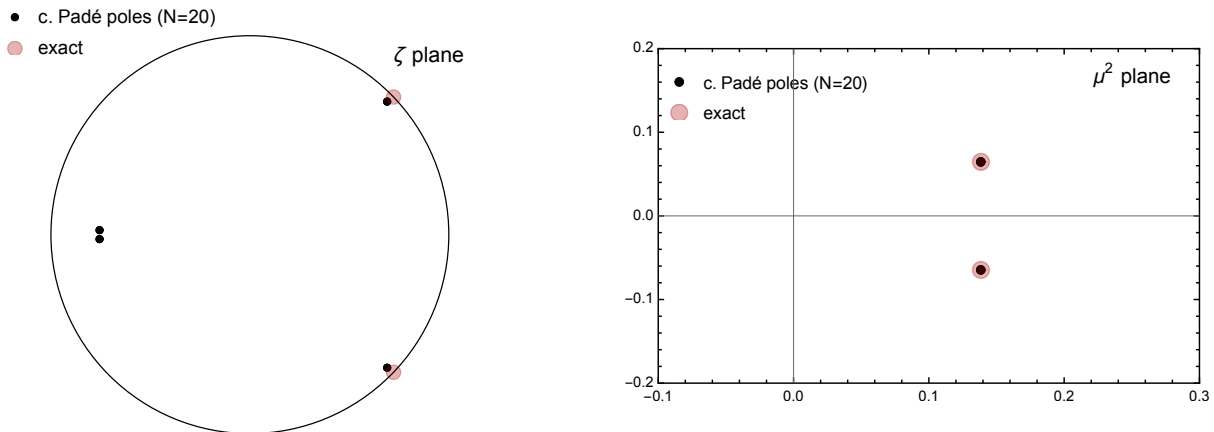


Figure 6: The poles of conformal Padé in the unit disk (left), and mapped back to the μ^2 plane (right). The conformal Padé method locates the physical LY singularities with high precision. These plots are made for $m_q = 0.1$ and $T = 0.9 \approx 1.34T_c$.

In Fig. 6 we show the singularities in the unit disk and in the μ^2 plane mapped via Eq. (21). Notice that compared with the exact result, the accuracy both in the unit disk and in the μ^2 plane is remarkable. This increase in precision can be quantified as a function of the number of terms [43]. Note that the conformal map (21) only requires knowledge of the *location* of the singularities, not of their exponent or strength. Therefore we can iterate this procedure to obtain even higher precision, which is particularly useful if only few coefficients are known (see the next section). Also notice that as opposed to Padé, there are no unphysical singularities along the real axis. This is due to the asymptotic form of the Padé polynomials, explained in [43].

In addition to the location of μ_{LY}^2 , the susceptibility can be reconstructed from the conformal Padé expression mapped back to the μ^2 plane:

$$\chi(T, \mu) \approx P[\chi(T, \phi(\zeta))]_{\zeta=\phi^{-1}(\mu^2)} \quad (24)$$

Note that apart from certain special rational values of θ , there is no analytic expression for the inverse function $\phi^{-1}(\mu^2)$, but it is straightforward to implement this inversion numerically. This procedure provides a significantly superior approximation to the susceptibility compared to ordinary Padé. This can be seen in Fig. 7, where we compare the conformal Padé results with other methods: Padé and the truncated Taylor expansion. The most dramatic improvement is in the range of validity of the extrapolation. The lack of unphysical poles along the real axis allows conformal Padé to provide a much better approximation to the susceptibility much further than the radius of convergence of the original Taylor series, $|\mu_{LY}^2|$. In particular,

the qualitative features of the higher order susceptibilities, such as the “peak-dip” structure of χ_3 , and the “peak-dip-peak” structure of χ_4 , are successfully reproduced even with a relatively small number of coefficients. These features cannot be seen in the truncated Taylor series, or in its Padé approximant. We stress that exactly the same input information (the coefficients $c_n(T)$) was used for these three approximations: this input data was simply processed differently, with the conformal Padé procedure being clearly superior.

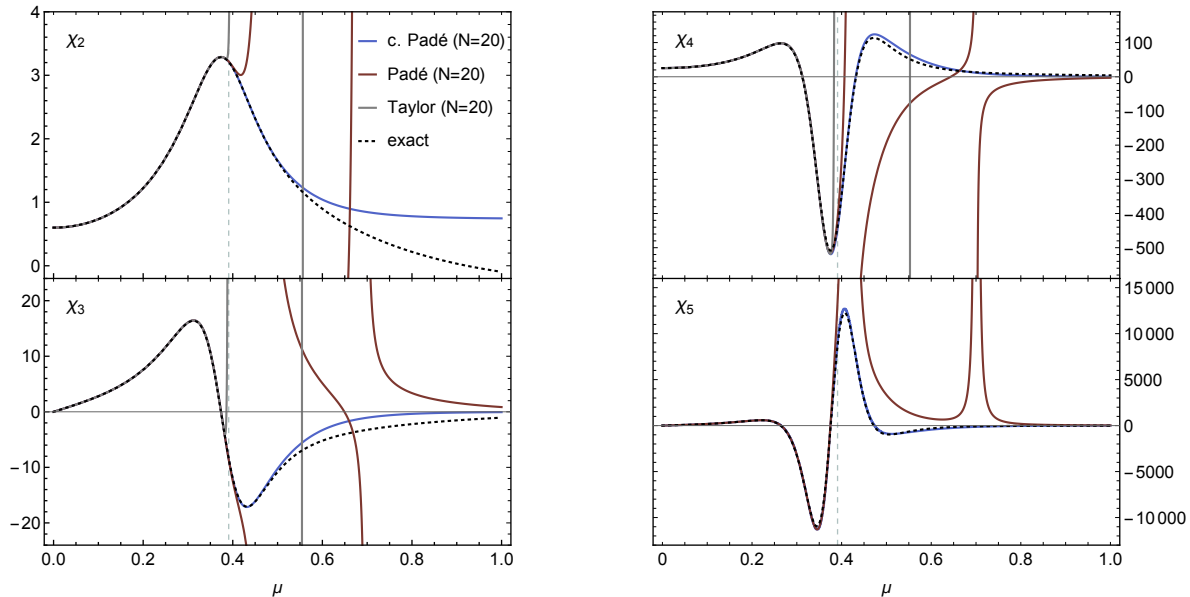


Figure 7: The susceptibilities χ_2, χ_3, χ_4 , and χ_5 for $m_q = 0.1$ and $T = 0.9 \approx 1.34T_c$ obtained from directly summing the truncated series expansion [gray], Padé [red] and conformal Padé [blue] resummations, compared with the exact result [black dashed]. The vertical dashed gray line denotes the radius of convergence $\mu = |\mu_{LY}| \approx 0.39$. Note that only the conformal Padé reconstruction is able to resolve the higher-order structure of the susceptibilities.

3.3 Reconstruction of the Lee-Yang trajectory

We repeated the procedure explained above for a range of temperatures to reconstruct the Lee Yang trajectory in Eq. (14), using the conformal Padé resummation. As mentioned earlier, the conformal map Eq. (21) contains μ_{LY} , the quantity we wish to compute from it. We therefore follow an iterative procedure which goes as follows:

1. Estimate a preliminary μ_{LY}^2 from ordinary Padé. This step does not involve the conformal map.
2. Plug this value in the conformal map, Eq. (21), and perform conformal Padé.
3. Update the value of μ_{LY}^2 extracted from conformal Padé.
4. Go to step 2 and repeat.

In steps 1 and 3, among the poles and zeros of Padé and conformal Padé we select the one that best approximates μ_{LY}^2 . This is achieved by filtering the poles and zeros to be stable under variation of the orders of the Padé polynomials. Then, the one with the largest imaginary part is selected from the filtered poles and zeros. If all poles and zeros are on the real axis, the one closest to the origin is selected.

The refined estimation $\mu_{EST}^2(T)$ so obtained may converge to outlying values for certain temperatures. To mitigate this uncertainty, a second-stage local optimization is performed by first fitting $\mu_{EST}^2(T)$ to the

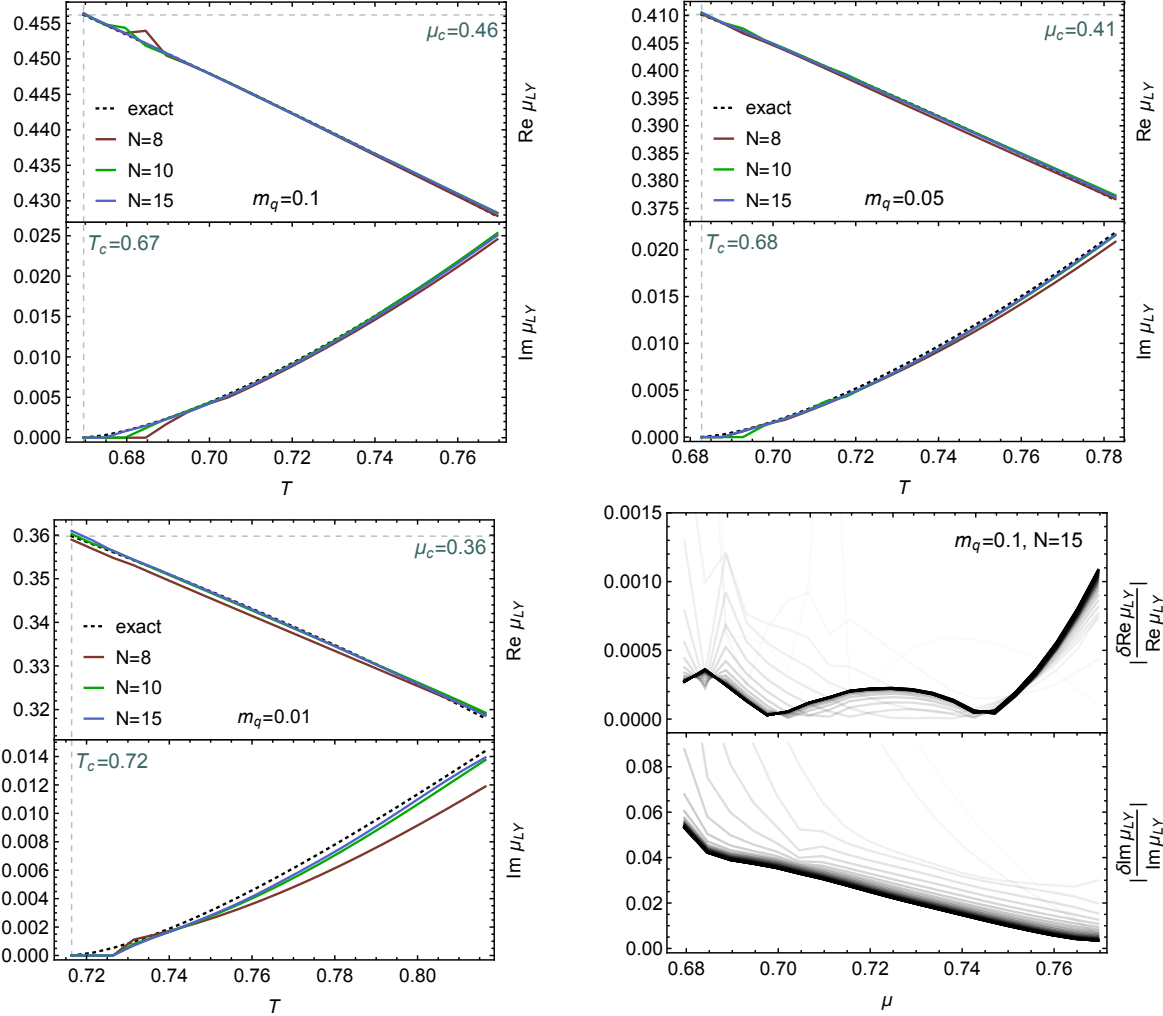


Figure 8: The Lee Yang trajectory (14) extracted from conformal Padé with different numbers of terms ($N = 8, 10, 15$), and with quark masses ($m_q = 0.1, 0.05, 0.01$), compared with the exact result. Bottom-right: The convergence of the iterative procedure (explained in text) with 30 iteration steps represented by the lines becoming darker.

formula in Eq. (14) (excluding obvious outliers) and inputting the fitted values $\mu_{FIT}^2(T)$ to the conformal map. A refined value for $\mu_{EST}^2(T)$ is then obtained by selecting the re-expanded Pade pole or zero closest to $\mu_{FIT}^2(T)$ in the μ^2 plane, and the whole process is repeated until convergence.

We used 30 steps for both stages of the iterative procedure. In Fig. 8 (top and bottom-left) we show the LY trajectory constructed by this procedure, for different values of m_q . In Fig. 8 (bottom-right) we show the convergence of the second-stage iterative procedure for $m_q = 0.1$ and $N = 15$. For visualization purposes the opacity of the curves is changed with the iteration step, becoming darker as the iterative procedure progresses. As seen from the Figure, we obtain the real part of the Lee-Yang singularity roughly with 0.02% accuracy. As expected, it is more difficult to resolve the imaginary part, as it vanishes at the critical point. However the accuracy is still at the percent level.

Note that even with just 8 terms in the initial expansion, the agreement with the exact result is quite good. The biggest challenge arises in the region very close $T = T_c$ where $\text{Im}\mu_{LY}$ approaches zero and resolving the small imaginary part becomes more difficult numerically. At the same time, as seen in Fig. 8, it is still possible to capture the $(T - T_c)^{3/2}$ behavior for $T \gtrsim T_c$ even for $N = 8$. This is in contrast to ordinary Padé which provides a poor resolution of $\text{Im}\mu_{LY}$ near T_c [11]. Finally by fitting the curves in Fig.

$m_q :$	0.1	0.05	0.01
T_c, μ_c (exact):	0.670, 0.456	0.683, 0.410	0.716, 0.360
T_c, μ_c ($N = 15$):	0.670, 0.456	0.684, 0.410	0.719, 0.360
T_c, μ_c ($N = 8$):	0.674, 0.455	0.683, 0.410	0.717, 0.359
K_1, K_2 (exact):	-0.267, 0.844	-0.308, 0.740	-0.362, 0.539
K_1, K_2 ($N = 15$):	-0.278, 0.831	-0.325, 0.719	-0.397, 0.526
K_1, K_2 ($N = 8$):	-0.282, 0.979	-0.334, 0.699	-0.400, 0.421

Table 1: The location of the critical point, (T_c, μ_c) , and the Ising mapping parameters, (K_1, K_2) of Eq. (9), obtained from the conformal Padé reconstruction of the LY trajectory, using $N = 15$ and $N = 8$ input coefficients in the initial expansion (14). For comparison we also list the exact values.

8 to the expected form of the trajectory, (14) T_c, μ_c , as well as the coefficients K_1 and K_2 . The results are given in Table 1. They are in good agreement with the exact results calculated directly from the mapping parameters (h_μ, h_T, r_μ, r_T) obtained via the Ginzburg-Landau analysis explained in Sec. 2.

4 Uniformization and analytic continuation of the Ising equation of state

In the previous section we showed how to extract highly accurate physical information about the Lee-Yang singularities from a finite-order polynomial approximation to the expansion of the partition function (or susceptibility) in powers of the chemical potential. In this section we discuss an even more difficult problem: how to extrapolate information in the high temperature region, $T > T_c$, to the low temperature region, $T < T_c$. This requires analytic continuation from the first Riemann sheet ($T > T_c$), where the original expansion is generated, across a cut to the next Riemann sheet, where $T < T_c$. We demonstrate that this can be achieved even when starting with a finite-order expansion, using methods developed in [12, 13]. This requires going beyond simple Padé analysis and conformal maps, instead using uniformizing maps which encode more information about branch cut structures. In this section we illustrate these ideas on the mean field Ising model and, in particular, show that the equation of state for low temperatures, $T < T_c$, can be constructed from the high temperature expansion at $T > T_c$ via analytic continuation. We first show that an *exact* uniformization is possible for the mean field Ising model, and then we show that even with partial information a simple uniformizing map enables accurate analytic continuation between Riemann sheets.

The key idea behind uniformization is to map the entire multi-sheeted domain of the original function to the upper half plane (it is useful to then map to the unit disk) in a specially chosen uniformizing variable [44, 45, 12, 13]. The net result is that different sheets are mapped to different regions of the unit disk, whose boundaries are connected by modular transformations. If the exact uniformizing map is known then this procedure is optimal and explicit [12, 13]. While it is rare in non-trivial physics problems to know the *exact* uniformizing map for the underlying Riemann surface, fortunately this uniformization procedure can also be implemented numerically using *approximate* information about the Riemann surface. For example, even an approximate uniformizing map, simply based on the locations of a few leading singularities, leads to dramatically higher precision on the first sheet, as well as the ability to cross approximately to other sheets [12, 13]. This use of approximate information about leading singularities is analogous to well-known procedures combining conformal maps with Padé analysis [35, 36, 37]. However, there is an important difference: with a conformal map one is limited to a given sheet, as the original sheet is mapped inside the whole unit disk. If instead one uses a uniformizing map to map first to the upper-half-plane and then into the unit disk, the first sheet is mapped to a particular region of the unit disk, and second sheet to another (connected) region, and so on. Therefore, analytic continuation trajectories in the unit disk can pass smoothly between sheets. In such a situation the uniformizing map is generically much more accurate than a corresponding conformal map, and dramatically more accurate than a Padé approximation.

Since the Ising model system has certain universal features, such as the existence of a dominant pair of complex conjugate singularities, even the mean field analysis can be used to develop suitable approximate

uniformizing maps which turn out to be significantly more accurate. We compare an exact uniformization of the mean field Ising system with an approximation based on a truncated initial expansion. The method is extremely simple to implement (see Section 4.2 below), and can in principle be adapted to more general problems, and beyond mean field.

4.1 Exact uniformization of the Ising model equation of state

Before discussing the analytic continuation through resummation of an approximate truncated expansion, let us briefly elaborate further on the analytic structure of the Ising equation of state. The naive solution $z = z(w)$ of the equation of state (8) produces three different expressions for $z(w)$ involving complicated cube roots. This reflects the fact that the solution to the equation of state is defined on a three-sheeted Riemann surface, which is in turn a direct consequence of truncating the action (5) at $\mathcal{O}(\phi^4)$.

However, as we show below, the mean field equation of state can also be solved in terms of a uniformizing variable, which makes the transition between sheets transparent.

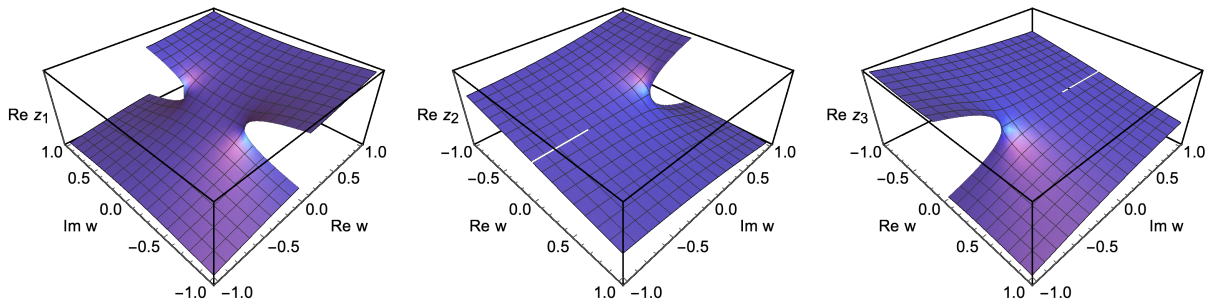


Figure 9: The solution $\text{Re}z(w)$ of the scaled equation of state (8) in the complex w plane. From left to right: $\text{Re}z_1(w)$, $\text{Re}z_2(w)$ and $\text{Re}z_3(w)$. Similar plots can be generated for the imaginary part.

To set notation, let us denote the three solutions of the scaled equation of state (8) as $z_1(w)$, $z_2(w)$ and $z_3(w)$, each defined over one of the sheets (see Fig. 9). Only two of the solutions are independent as $z_3(w) = -z_2(-w)$. We will refer to the sheets over which $z_1(w)$ and $z_2(w)$ are defined as the high T and low T sheets, respectively. The high T sheet captures the equation of state for $r = (T - T_c)/T_c > 0$ (see Fig. 10, left). It has two branch cuts emanating from branch points at $w = \pm 2i/(3\sqrt{3})$, which correspond to the Lee-Yang edge singularities where $dw/dz = 0$. The other two sheets over which $z_2(w)$ and $z_3(w)$ are defined capture the low temperature, $T < T_c$, behavior where $r < 0$. They are related to each other by the reversal of the direction of the magnetic field, h , i.e. $w \rightarrow -w$. The low T sheets each have a single branch point, at $z = \pm 2i/(3\sqrt{3})$, respectively. Furthermore one can move from the high T sheet to the low T sheet via the analytic continuation: $r \rightarrow e^{-i\pi}r$, which corresponds to $w \rightarrow e^{3i\pi/2}w$ and $z \rightarrow e^{i\pi/2}$. The equation of state, $M(h)$ for $T > T_c$ and $T < T_c$ is shown in Fig. 10, in terms of the scaling variables z and w . For $T > T_c$ the physical (i.e. real) values of magnetization and magnetic field correspond to $\text{Re}z_1$ and $\text{Re}w$, respectively. For $T < T_c$ and $h < 0$, after analytic continuation we obtain $M \propto -\text{Im}z_2$. Similarly for $T < T_c$ and $h > 0$ we have $M \propto -\text{Im}z_3$.

Let us now suppose that we only have access to a finite number of terms of the Taylor series expansion of the equation of state around $h = 0$, for various fixed values of $T > T_c$. This corresponds to having a finite number of terms of the Taylor series expansion of $z_1(w)$ around $w = 0$:

$$z_1(w) = w - w^3 + 3w^5 - 12w^7 + 55w^9 + \dots \quad (25)$$

This series has a radius of convergence $|w_{LY}| = \frac{2}{3\sqrt{3}} \approx 0.385$, determined by the nearest singularities to the origin on the first sheet, which are the Lee-Yang singularities. Therefore an approximation to the equation of state with a truncated Taylor series can only capture a limited range $w < |w_{LY}|$, regardless of how

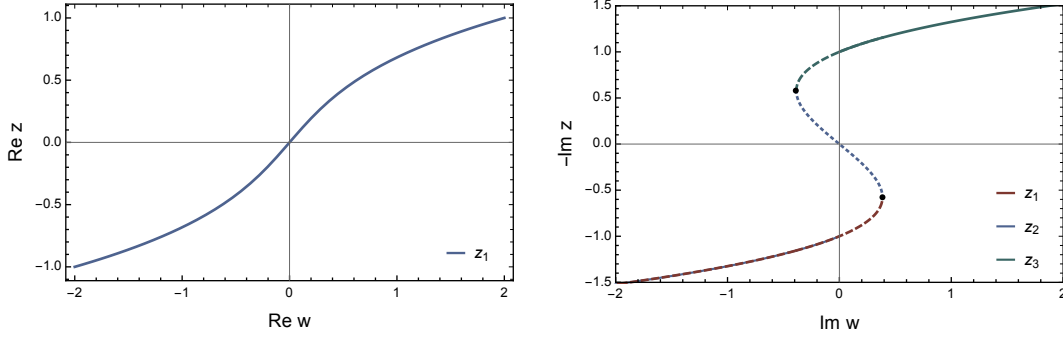


Figure 10: The scaled equation of state $z(w)$ for $T > T_c$ (left) and $T < T_c$ (right). The black dots in the right-hand figure show the location of the Lee-Yang singularities $w = \pm \frac{2i}{3\sqrt{3}}$ which corresponds to the spinodal point. The dashed/dotted parts denote the meta-stable and unstable regions, respectively.

many terms we have in the expansion. To continue beyond the radius of convergence we can make a Padé approximant of the truncated Taylor series. As shown in Figure 11, this leads to an improvement in the direction of $\text{Re} w$, along which there are no singularities (the Lee-Yang singularities lie on the $\text{Im} w$ line).

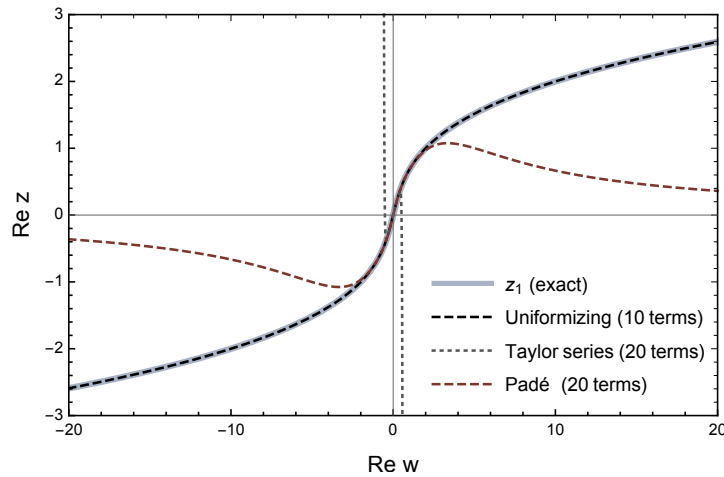


Figure 11: The scaled equation of state $z(w)$ for $T > T_c$, shown as the analytic continuation of finite truncations of the Taylor expansion for $z_1(w)$ on the first sheet in (25). The truncated Taylor series [dotted line] is limited by the radius of convergence, which is determined by the Lee-Yang singularities: $|w_{LY}| \approx 0.385$. A Padé approximation [red dashed line] extends accurately for some distance beyond the radius of convergence, but with the uniformizing map [black dashed line] in (33) the agreement with the exact expression is dramatically more accurate, extending much further. Furthermore, this uniformized analytic continuation was generated with half the number of terms of the initial expansion.

However, Padé breaks down along the imaginary w direction because it places poles along the imaginary axis in an attempt to represent the branch cuts. Recall that the Padé approximant is a *rational* function so its only singularities are poles. Padé represents a branch cut as an arc of interlacing poles and zeros accumulating to the associated branch point [33, 12, 13]. This has the consequence that the Padé approximant is not accurate near a cut, and thus does not accurately describe the analytic continuation across a cut. Therefore, the Padé approximant to the truncated equation of state $z = z(w)$, which was developed on the $T > T_c$ sheet, cannot be accurately continued to the $T < T_c$ sheets.

This inherent deficiency of Padé can be overcome by *first* using a uniformization map, and *then* making a Padé approximation [12, 13]. For the three-sheeted cubic in (8) this can be done exactly, using the following basic facts:

1. The equation of state (8) is naturally solved in terms of hypergeometric functions (see (26)-(29)), whose analytic continuation properties are well-defined and simple.
2. The hypergeometric functions are uniformized by an explicit mapping to the upper half plane (see (30)), which can then be mapped into the unit disk (see (32)). The resulting uniformization (33) then covers all sheets, which can be accessed simply by moving around in the disk. See Figures 12,13, and [46] for an interactive realization.

The physical implication is two-fold. First, the resulting analytic continuation, starting with exactly the same truncated expansion, is dramatically more accurate, especially near the singularities and cuts. Second, different sheets in the original variable are mapped to different regions in the uniformizing upper half plane, but the result is analytic in the entire upper half plane (or in the entire unit disk), and therefore can be analytically continued between sheets. To make this construction explicit, we first note that the equation of state (8) is solved by

$$z_1(w) = w {}_2F_1\left(\frac{2}{3}, \frac{1}{3}, \frac{3}{2}; -\frac{27w^2}{4}\right) \quad (26)$$

$$z_2(w) = -\frac{w}{2} {}_2F_1\left(\frac{2}{3}, \frac{1}{3}, \frac{3}{2}; -\frac{27w^2}{4}\right) + i {}_2F_1\left(\frac{1}{6}, -\frac{1}{6}, \frac{1}{2}; -\frac{27w^2}{4}\right). \quad (27)$$

and we recall that $z_3(w) = -z_2(-w)$. Furthermore, we can linearize the argument using standard hypergeometric identities (see 15.8.27 and 15.8.28 in [47]):

$$z_1(w) = -\frac{2i}{\sqrt{3}} \left[{}_2F_1\left(\frac{1}{3}, -\frac{1}{3}, \frac{1}{2}; \frac{1}{2}(1-i\tilde{w})\right) - {}_2F_1\left(\frac{1}{3}, -\frac{1}{3}, \frac{1}{2}; \frac{1}{2}(1+i\tilde{w})\right) \right] \quad (28)$$

$$z_2(w) = \frac{2i}{\sqrt{3}} {}_2F_1\left(\frac{1}{3}, -\frac{1}{3}, \frac{1}{2}; \frac{1}{2}(1-i\tilde{w})\right). \quad (29)$$

Here we define the rescaled variable $\tilde{w} := \frac{3\sqrt{3}}{2}w$, in terms of which the Lee-Yang singularities are normalized to be at $\tilde{w} = \pm i$. Expressed in this form, all the branch cut technicalities are greatly simplified because the hypergeometric functions have simple connection formulae across a cut [44].

The next step is the crucial one. We use the fact that hypergeometric functions are uniformized by the elliptic modular function $\lambda(\tau)$, where τ lives in the upper half plane $\text{Im}\tau > 0$ [44]. This is implemented by the following transformation (to simplify the formulas we use the rescaled variable $\tilde{w} := \frac{3\sqrt{3}}{2}w$):

$$\tilde{w}(\tau) = i(-1 + 2\lambda(\tau)) \quad \text{with inverse} \quad \tau(\tilde{w}) = i \frac{\mathbb{K}\left(\frac{1+i\tilde{w}}{2}\right)}{\mathbb{K}\left(\frac{1-i\tilde{w}}{2}\right)} \quad (30)$$

Here $\lambda(\tau)$ is the modular lambda function $\lambda(\tau) = \theta_2^4(\tau)/\theta_3^4(\tau)$, where $\theta_2(\tau)$ and $\theta_3(\tau)$ are the Jacobi elliptic functions: $\theta_2(\tau) = \sum_{n=-\infty}^{\infty} e^{2\pi i\tau(n+1/2)^2}$ and $\theta_3(\tau) = \sum_{n=-\infty}^{\infty} e^{2\pi i\tau n^2}$, defined in the upper half plane $\text{Im}\tau > 0$. The function $\mathbb{K}(m)$ in (30) is the complete elliptic integral of the first kind:

$$\mathbb{K}(m) = \int_0^{\pi/2} \frac{d\theta}{\sqrt{1 - m \sin^2 \theta}} \quad (31)$$

The functions $\lambda(\tau)$ and $\mathbb{K}(m)$ are implemented in Mathematica as `ModularLambda` and `EllipticK`.

It is convenient for both numerical and visualization purposes to combine this map with a subsequent map that takes the upper half τ plane into the unit disk $|\zeta| < 1$:

$$\tau(\zeta) := i \left(\frac{1+i\zeta}{1-i\zeta} \right) \quad \text{with inverse} \quad \zeta = i \left(\frac{1+i\tau}{1-i\tau} \right) \quad (32)$$

The combined transformation, from the three-sheeted w plane directly to the unit disk in ζ is:

$$\tilde{w} = i \left[-1 + 2\lambda \left(i \frac{1+i\zeta}{1-i\zeta} \right) \right] \quad \text{with inverse} \quad \zeta = i \frac{\mathbb{K}\left(\frac{1-i\tilde{w}}{2}\right) - \mathbb{K}\left(\frac{1+i\tilde{w}}{2}\right)}{\mathbb{K}\left(\frac{1-i\tilde{w}}{2}\right) + \mathbb{K}\left(\frac{1+i\tilde{w}}{2}\right)} \quad (33)$$

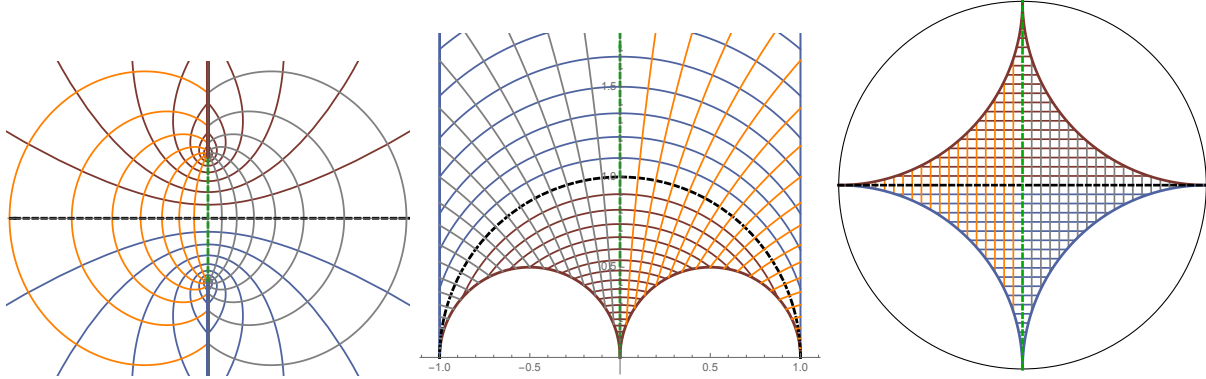


Figure 12: Left: The \tilde{w} plane for the first sheet (the high T sheet, $T > T_c$). The red and blue (upper/lower) lines denote the branch cuts emanating from the LY singularities at $\tilde{w} = \pm i$. Center: The modular τ plane after the map $\tilde{w} \rightarrow \tau$ in (30). Right: The unit disk (the ζ plane) after the map $\tau \rightarrow \zeta$ in (32). The curves with different colors represent the mapping between the w, τ and ζ planes.

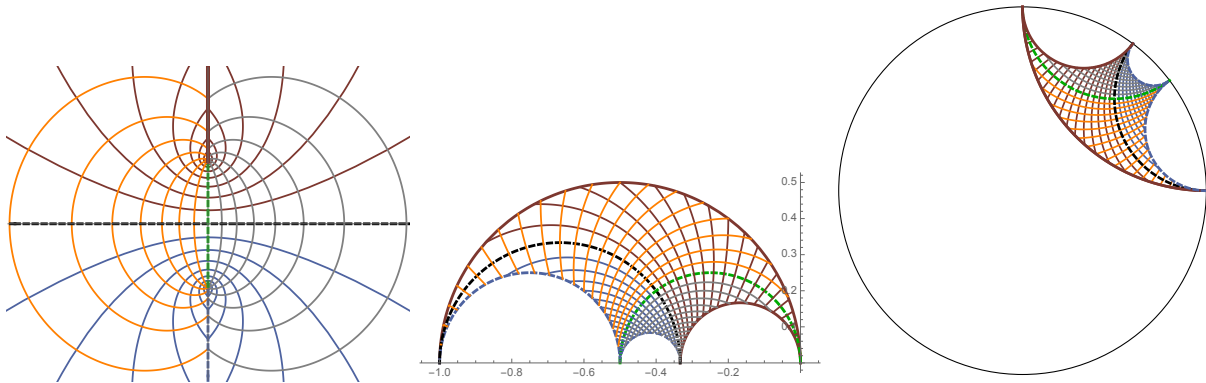


Figure 13: The representations of the second sheet (the low T sheet, $T < T_c$) in the \tilde{w} plane (left), in the modular τ plane (center), and in the ζ unit disk (right). Note that the low T sheet maps to regions in τ and ζ that connect directly to regions associated with the first sheet, shown in Figure 12.

The geometrical properties of these maps are depicted in Figures 12, 13 and 14. Figure 12 shows how the first sheet in the \tilde{w} variable is mapped to a specific region of the upper half complex τ plane, and subsequently to a specific "circular quadrilateral" region of the unit disk in the ζ variable (right-hand plot in Figures 12). Figure 13 shows how the second sheet in the \tilde{w} variable is mapped to a different but connected portion of the upper half τ plane, and correspondingly to a different but connected portion of the unit disk in the ζ variable. These two regions are related by a modular transformation. This can be continued *ad infinitum*, with the trajectories in the unit disk in ζ encoding all possible trajectories on the three-sheeted Riemann surface in the \tilde{w} variable. Examples are given below, and see [46] for an interactive realization.

4.2 Approximate Reconstruction of the Ising Equation of State: the Uniformized-Padé Method

The maps described in the previous section give an *exact* uniformization of $z(w)$ on its entire Riemann surface. However, the main practical use of these maps is as building blocks for *approximate* uniformizing maps. For example, suppose we know (or conjecture) that a finite-order expansion about the origin is limited by two dominant singularities, which are in general branch points.⁵ Then an approximate uniformizing map can be used, based solely on this (conjectured) information. If the two branch points are symmetrically

⁵This is a common occurrence in physical applications: e.g. [36, 48, 40, 41, 49, 42].

located, then the map is precisely (33), but the corresponding map is known when these two dominant singularities have general locations [38, 39, 12, 13].

Now suppose we do not have the exact solutions $z_1(w)$ and $z_2(w)$ of the scaled equation of state (8), but just a finite-order truncated expansion for $z_1(w)$, generated in the high temperature region. We first locate the singularities that limit the convergence: this can be done approximately, using for example methods described in Section 3 (or even more accurate methods in [12, 13]). We learn that there are two dominant singularities. Let us rescale the variable w to place these at $\tilde{w} = \pm i$.

The actual implementation of the reconstruction method is extremely simple. We note that the map from \tilde{w} to ζ in (33) takes the origin $\tilde{w} = 0$ to the origin of the disk, $\zeta = 0$:

$$\begin{aligned}\tilde{w}(\zeta) &= i \left[-1 + 2\lambda \left(i \frac{1+i\zeta}{1-i\zeta} \right) \right] \\ &= \frac{\pi^2 \zeta}{\Gamma\left(\frac{3}{4}\right)^4} + \frac{1}{4} \left(\frac{\pi^2 \zeta}{\Gamma\left(\frac{3}{4}\right)^4} \right)^3 + \frac{13}{240} \left(\frac{\pi^2 \zeta}{\Gamma\left(\frac{3}{4}\right)^4} \right)^5 + \dots\end{aligned}\quad (34)$$

This means that we simply compose the series expansions to convert the finite-order expansion in \tilde{w} into a finite-order expansion in ζ . We then Padé in ζ and map back to \tilde{w} . The resulting Uniformized-Padé procedure is [12, 13]:

1. Re-expand the original truncated Taylor series in \tilde{w} as a Taylor series in ζ , and truncate at the same order in ζ . This procedure is optimal [12].
2. Make a Padé approximant of the resulting truncated series in terms of ζ .
3. Map this Padé approximant back to the \tilde{w} plane using the inverse map in (33). (Note that in contrast with the case of the conformal map (21), here the uniformizing map and its inverse are both explicit.)

The output of this simple algorithm is an analytic continuation of the the truncated expansion of $z_1(w)$, which is of high precision on the first (high temperature) sheet, and which smoothly crosses to other sheets, in particular to the low temperature region. The high precision also means that the procedure can be iterated to refine an initial estimate of the singularity locations.

4.2.1 Improved accuracy on the high temperature sheet

To quantify the high precision of this Uniformized-Padé analytic continuation on the first ($T > T_c$) sheet, we compare it in Figure 11 with the exact expression for $z_1(w)$ in (26) (or (28)), with the Taylor expansion of $z_1(w)$ truncated after 20 terms, and with the (near diagonal) Padé approximant of this 20-term truncated expansion. As expected, the truncated series breaks down at the Lee-Yang radius of convergence $\frac{2}{3\sqrt{3}} \approx 0.385$. The Padé approximant is better, going beyond the radius of convergence, but it breaks down at $\text{Re} w \approx \pm 2$. By comparison, the Uniformized-Padé approximation matches very accurately the exact result for $z_1(w)$ all the way out to $\text{Re} w = \pm 20$, well beyond the Lee-Yang radius of convergence. Furthermore, this Uniformized-Padé approximation was implemented using half the number of input terms. This higher precision shown in Figure 11 is along the $\text{Re} w$ axis, which does not encounter any singularities or cross any cuts. The improvement is even more dramatic along the imaginary w axis, where Padé fails already at the radius of convergence, where it first encounters the branch points.

Note that the construction of the uniformizing map in (33) uses knowledge of the location of the Lee-Yang singularities. As discussed in Section 3, if these locations are unknown they can be found numerically to high precision by iteration [12, 13]. The fact that the uniformizing map (33) leads to an *exact* uniformization of the function relies on the underlying Riemann surface being that associated with the hypergeometric functions, which solve the equation of state (8). However, even if it were not the exact Riemann surface, the use of this uniformizing map produces significantly higher precision than other methods for any problem with a pair of leading singularities [12, 13], which is a common occurrence in a wide range of physical applications.

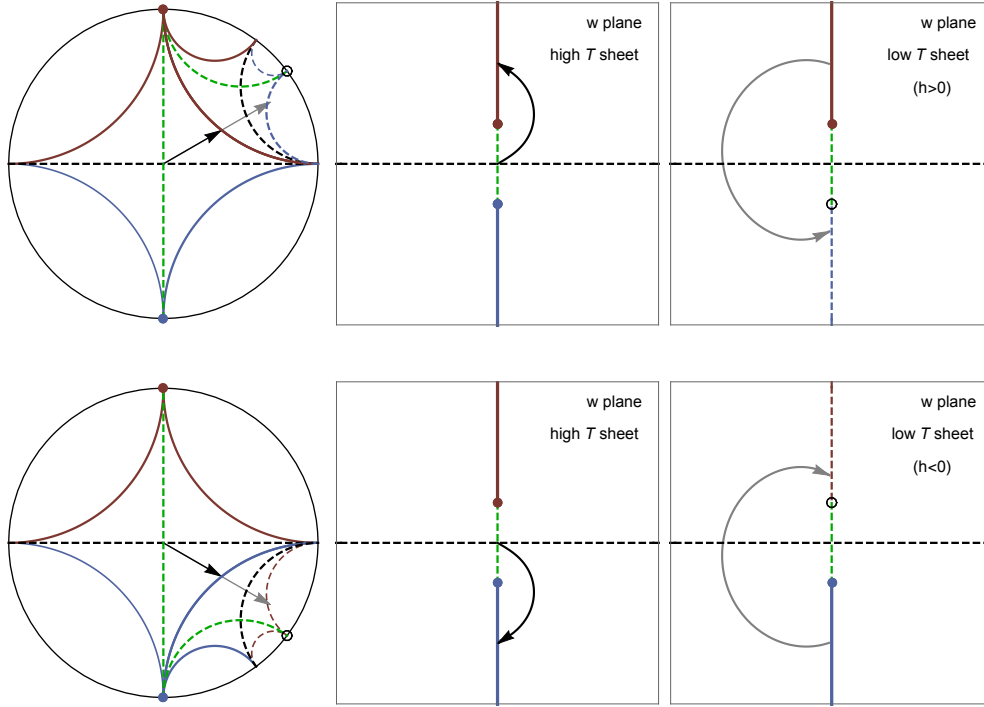


Figure 14: The analytic continuation from the high T sheet to the low T sheets with $h > 0$ (upper) and $h < 0$ (lower). The arrows showing trajectories inside the unit disk match the trajectories that cross from the high T sheet to the low T sheet in the w variable. The corresponding boundaries of the sheets (i.e. the edges of the cuts) become circular boundaries inside the unit disk, obtained by Schwarz reflections.

4.2.2 Analytic continuation from the high temperature sheet to the low temperature sheets

In addition to improved accuracy on the first sheet, a distinguishing feature of the Uniformized-Padé approximation is its ability to reconstruct the underlying function globally, making it possible to pass to higher Riemann sheets, even when starting from a finite-order truncated approximation [12, 13]. This can be seen already in the behavior of the approximation along the imaginary w axis, which encounters the Lee-Yang singularities at $\tilde{w} = \pm i$, and the associated branch cuts that need to be crossed in order to pass from the high temperature sheet to the low temperature sheets.

The transition from one sheet to another works as follows. Consider the physical problem of trying to evaluate the low temperature equation of state starting from a truncated expansion of the high temperature equation of state. This (truncated) high temperature expansion is generated on the first sheet, but we want the solution on the second (low T) sheet. As shown in Figure 12, the uniformizing map takes the first sheet to a circular quadrilateral inside the unit disk, for the ζ variable. Suppose we cross to the low T branch by crossing the upper branch cut (shown in red). The low T sheet in this case is represented in the unit disk as a region obtained by performing a Schwarz reflection with respect to the image of the branch cut in the unit circle i.e. the upper right red circle in Fig. 12 (right). The image of the low T sheet obtained this way is shown in Fig. 13 (right). In the modular plane this corresponds to a particular Möbius transformation which maps the image of the first sheet in Fig. 12 (center) inside the region bounded by the the semicircle (see Fig. 13 (center)). Notice that in this low T sheet (where $h < 0$), there is only one branch cut, shown in solid red. As opposed to the high T sheet, the line segment $\text{Im}w < -2/(3\sqrt{3})$ is not a branch cut and is therefore shown as a dashed blue line in Fig. 13. In fact this is the region where the physical equation of state for $T < T_c$ and $h > 0$ is defined, namely the magnetization $M \propto -\text{Im}w$ with $\text{Im}w < -2/(3\sqrt{3})$.

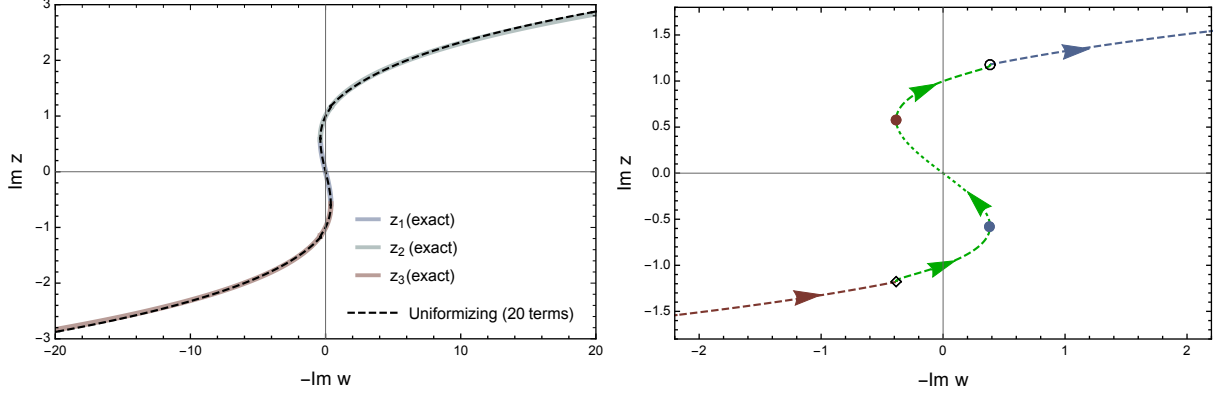


Figure 15: The low T equation of state, in terms of the scaled variables z and w , reconstructed from the high T expansion using uniformed Padé, compared with the exact result (left). Note that with just 20 input terms for the expansion of $z_1(w)$ on the high T sheet we can reconstruct the solution on other sheets with high precision. The right-hand panel shows a zoomed-in view, highlighting the trajectory in the w plane and in the unit disk, as shown in Fig. 16.

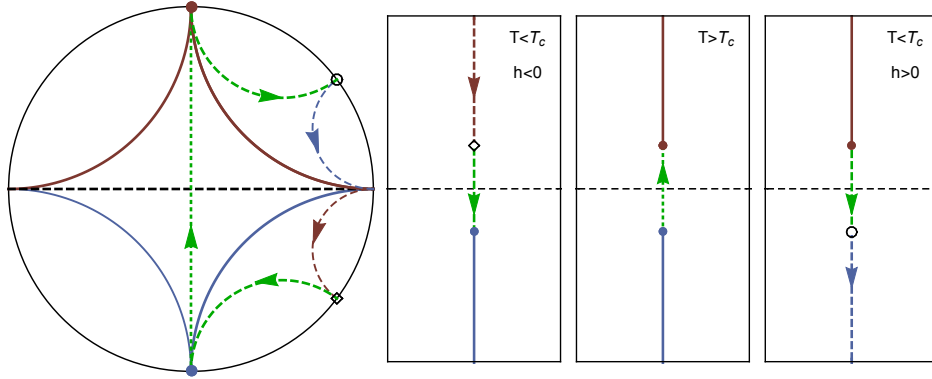


Figure 16: The trajectory that captures the low T equation of state $M(h)$ in the scaling variables in the unit disk (left) and in the w plane (right). The trajectory goes through three different Riemann sheets (right) in the w plane but is smooth and entirely contained in the unit disk (left).

This is illustrated in Figure 14, which shows how the continuation from the high temperature sheet to the low temperature sheet appears in the unit disk. An illustrative trajectory in the w plane that goes from the high T branch to the low T branch and its image on the unit disk are shown in Fig. 14. This trajectory, in the w plane, starts from the origin, crosses the upper branch cut to the low T sheet and finally ends at some point on the negative imaginary axis with $\text{Im}w < -2/3\sqrt{3}$, which is proportional to some value of the magnetization with $T < T_c$ and $h > 0$ in the stable branch of the equation of state. In the unit disk, this trajectory is a line segment shown in Fig. 14 (top). The main point we emphasize is that even though in the w plane the trajectory goes through different sheets, in the unit disk it is completely regular. Similarly, it is also possible to analytically continue to the $h < 0$ sheet by going through the lower branch cut (blue line in Fig. 12, left) as shown in Fig. 14 (bottom).

Figures 15 and 16 show how the low temperature equation of state can be reconstructed from just 20 input terms of the Taylor expansion of the high temperature equation of state. In Fig. 15 (left) we compare the exact result with the result obtained from the uniformized-Padé approximation. Similar to the high T expansion in Figure 11, the numerical accuracy in the low T region is also remarkable and extends to large values $|w| \approx 20$. We stress that this result is obtained from the Taylor expansion of $z_1(w)$ for $T > T_c$ and analytically continued via the uniformizing map. It is not the expansion of $z_2(w)$ or $z_3(w)$. Nevertheless it captures the low T behavior of the equation of state remarkably well in a region where neither the truncated

Taylor series nor the Padé approximant has any applicability whatsoever.

5 Summary and Conclusions

In this paper we described a robust framework to reconstruct efficiently the equation of state of a thermodynamic system near a critical point T_c, μ_c , using only a finite number of coefficients from a local expansion at $\mu = 0$. We first showed that pairing the usual Padé resummation with a conformal map significantly improves the approximation to the underlying equation of state, compared to simply summing the truncated Taylor series or performing a regular Padé approximation. The most important improvement is the extension of the range of the approximation. The applicability of the Taylor series is limited by its radius of convergence. Ordinary Padé resummation allows one to go past beyond the radius of convergence but produces unphysical singularities which limit the improvement in physically important regions. Conformal Padé eliminates these unphysical singularities which leads to a dramatic improvement in the range of the approximation. In particular we showed (see Figure 7) that it captures the characteristic features of the susceptibilities in the vicinity of the critical point which play a significant role in the search for the QCD critical point.

We also showed that it is even possible to analytically continue to higher Riemann sheets by pairing Padé resummation with a suitably engineered map, namely a uniformizing map. We demonstrated this procedure in the Ising model. Physically, this makes it possible to analytically continue an expansion obtained in the high T crossover region ($r > 0$) to the low T first-order region ($r < 0$). The only input we needed was the Taylor coefficients and the location of the Lee-Yang singularity whose value can be approximated by the same iteration procedure explained in Sec. 3.

There are various future directions left for future work. An important extension is to go beyond the mean field limit. For the Ising model, in the crossover region ($r > 0$), which corresponds to the first sheet, the two-cut nature of the w plane is universal [16] albeit with different branch point singularities determined by the critical exponents, $\beta\delta$. Given that the $r < 0$ region has more structure, such as the Langer cut [21, 22, 23], it would be interesting to extend this machinery beyond the mean field. Beyond the mean field approximation, even though in general the equation of state does not have an analytic representation, knowledge of the universality class and/or the critical exponents can help to construct an *approximate* uniformizing map that enables improved analytic continuation. Another interesting aspect of beyond the mean field case is that the equation of state, $w = F(z)$, can be expressed as an ϵ expansion which is asymptotic. Related conformal Padé techniques are well known in the study of the ϵ expansion [50, 35]. One could construct a hybrid resummation scheme that involves uniformizing and conformal Padé both in z and the Borel plane of ϵ . Alternatively one could use the parametric representation of the equation of state [51]. Another possible direction is to incorporate the analytical continuation scheme introduced in this paper with the expansions obtained with pure imaginary chemical potential, as for QCD it is very challenging to compute beyond the first few terms of the Taylor expansion with real μ . Finally it is also necessary to address the issue of noise in the Taylor coefficients as they are typically computed via stochastic methods which unavoidably introduces noise. It is therefore important to ensure the stability of these resummation methods with noisy data.

Acknowledgments

This work is supported in part by the U.S. Department of Energy, Office of High Energy Physics, Award DE-SC0010339 (GD) and the Junior Faculty Development Award from UNC-CH (GB). We thank Ovidiu Costin for discussions.

References

- [1] A. Bzdak, S. Esumi, V. Koch, J. Liao, M. Stephanov, and N. Xu, “Mapping the Phases of Quantum Chromodynamics with Beam Energy Scan,” *Phys. Rept.* **853** (2020) 1–87, [arXiv:1906.00936 \[nucl-th\]](#).
- [2] X. An, M. Bluhm, L. Du, G. V. Dunne, C. Gale, J. Grefa, U. Heinz, A. Huang, J. M. Kartheim, D. E. Kharzeev, V. Koch, J. Liao, S. Li, M. Martinez, M. McNelis, D. Mroczek, S. Mukherjee, M. Nahrgang,

- A. N. Acuna, J. Noronha-Hostler, D. Oliinychenko, P. Parotto, I. Portillo, M. S. Pradeep, S. Pratt, K. Rajagopal, C. Ratti, G. Ridgway, T. Schaefer, B. Schenke, C. Shen, S. Shi, M. Singh, V. Skokov, D. T. Son, A. Sorensen, M. Stephanov, R. Venugopalan, V. Vovchenko, R. Weller, H.-U. Yee, and Y. Yin, “The best framework for the search for the qcd critical point and the chiral magnetic effect,” 2021.
- [3] A. Bazavov *et al.*, “The QCD Equation of State to $\mathcal{O}(\mu_B^6)$ from Lattice QCD,” *Phys. Rev. D* **95** no. 5, (2017) 054504, [arXiv:1701.04325 \[hep-lat\]](#).
- [4] C. Ratti, “Lattice QCD and heavy ion collisions: a review of recent progress,” *Rept. Prog. Phys.* **81** no. 8, (2018) 084301, [arXiv:1804.07810 \[hep-lat\]](#).
- [5] S. Borsányi, Z. Fodor, J. N. Guenther, R. Kara, S. D. Katz, P. Parotto, A. Pásztor, C. Ratti, and K. K. Szabó, “Lattice QCD equation of state at finite chemical potential from an alternative expansion scheme,” [arXiv:2102.06660 \[hep-lat\]](#).
- [6] S. Mondal, S. Mukherjee, and P. Hegde, “Lattice qcd equation of state for nonvanishing chemical potential by resumming taylor expansion,” 2021.
- [7] S. Mukherjee, F. Rennecke, and V. V. Skokov, “Analytical structure of the equation of state at finite density: Resummation versus expansion in a low energy model,” [arXiv:2110.02241 \[hep-ph\]](#).
- [8] P. Dimopoulos, L. Dini, F. Di Renzo, J. Goswami, G. Nicotra, C. Schmidt, S. Singh, K. Zambello, and F. Ziesché, “A contribution to understanding the phase structure of strong interaction matter: Lee-Yang edge singularities from lattice QCD,” [arXiv:2110.15933 \[hep-lat\]](#).
- [9] **Bielefeld-Parma** Collaboration, S. Singh, P. Dimopoulos, L. Dini, F. Di Renzo, J. Goswami, G. Nicotra, C. Schmidt, K. Zambello, and F. Ziesche, “Lee-Yang edge singularities in lattice QCD : A systematic study of singularities in the complex μ_B plane using rational approximations,” in *38th International Symposium on Lattice Field Theory*. 11, 2021. [arXiv:2111.06241 \[hep-lat\]](#).
- [10] M. A. Stephanov, “QCD phase diagram and the critical point,” *Prog. Theor. Phys. Suppl.* **153** (2004) 139–156, [arXiv:hep-ph/0402115](#).
- [11] G. Basar, “Universality, lee-yang singularities, and series expansions,” *Phys. Rev. Lett.* **127** (Oct, 2021) 171603. <https://link.aps.org/doi/10.1103/PhysRevLett.127.171603>.
- [12] O. Costin and G. V. Dunne, “Uniformization and Constructive Analytic Continuation of Taylor Series,” [arXiv:2009.01962 \[math.CV\]](#).
- [13] O. Costin and G. V. Dunne, “Conformal and Uniformizing Maps in Borel Analysis,” *Eur. Phys. J. ST* **230** (2021) 2679–2690, [arXiv:2108.01145 \[hep-th\]](#).
- [14] M. A. Halasz, A. D. Jackson, R. E. Shrock, M. A. Stephanov, and J. J. M. Verbaarschot, “Phase diagram of qcd,” *Physical Review D* **58** no. 9, (Sep, 1998) . <http://dx.doi.org/10.1103/PhysRevD.58.096007>.
- [15] M. S. Pradeep and M. Stephanov, “Universality of the critical point mapping between Ising model and QCD at small quark mass,” *Phys. Rev. D* **100** no. 5, (2019) 056003, [arXiv:1905.13247 \[hep-ph\]](#).
- [16] T. D. Lee and C.-N. Yang, “Statistical theory of equations of state and phase transitions. 2. Lattice gas and Ising model,” *Phys. Rev.* **87** (1952) 410–419.
- [17] M. Halasz, A. Jackson, and J. Verbaarschot, “Yang-lee zeros of a random matrix model for qcd at finite density,” *Physics Letters B* **395** no. 3-4, (Mar, 1997) 293–297. [http://dx.doi.org/10.1016/S0370-2693\(97\)00015-4](http://dx.doi.org/10.1016/S0370-2693(97)00015-4).
- [18] M. A. Stephanov, “QCD critical point and complex chemical potential singularities,” *Phys. Rev. D* **73** (2006) 094508, [arXiv:hep-lat/0603014](#).

- [19] S. Mukherjee and V. Skokov, “Universality driven analytic structure of the QCD crossover: radius of convergence in the baryon chemical potential,” *Phys. Rev. D* **103** no. 7, (2021) L071501, [arXiv:1909.04639 \[hep-ph\]](#).
- [20] M. E. Fisher, “Yang-Lee Edge Singularity and ϕ^3 Field Theory,” *Phys. Rev. Lett.* **40** (1978) 1610–1613.
- [21] X. An, D. Mesterházy, and M. A. Stephanov, “Functional renormalization group approach to the Yang-Lee edge singularity,” *JHEP* **07** (2016) 041, [arXiv:1605.06039 \[hep-th\]](#).
- [22] X. An, D. Mesterházy, and M. A. Stephanov, “On spinodal points and Lee-Yang edge singularities,” *J. Stat. Mech.* **1803** no. 3, (2018) 033207, [arXiv:1707.06447 \[hep-th\]](#).
- [23] X. An, D. Mesterházy, and M. A. Stephanov, “Critical fluctuations and complex spinodal points,” *PoS CPOD2017* (2018) 040.
- [24] P. H. Damgaard and U. M. Heller, “On spin and matrix models in the complex plane,” *Nucl. Phys. B* **410** (1993) 494–520, [arXiv:hep-lat/9307016](#).
- [25] S. Ejiri, “Lee-Yang zero analysis for the study of QCD phase structure,” *Phys. Rev. D* **73** (2006) 054502, [arXiv:hep-lat/0506023](#).
- [26] M. Wakayama, V. Bornyakov, D. Boyda, V. Goy, H. Iida, A. Molochkov, A. Nakamura, and V. Zakharov, “Lee-yang zeros in lattice qcd for searching phase transition points,” *Physics Letters B* **793** (2019) 227–233. <https://www.sciencedirect.com/science/article/pii/S0370269319302734>.
- [27] A. Connelly, G. Johnson, S. Mukherjee, and V. Skokov, “Universality driven analytic structure of QCD crossover: radius of convergence and QCD critical point,” *Nucl. Phys. A* **1005** (2021) 121834, [arXiv:2004.05095 \[hep-ph\]](#).
- [28] C. Schmidt, J. Goswami, G. Nicotra, F. Ziesché, P. Dimopoulos, F. Di Renzo, S. Singh, and K. Zambello, “Net-baryon number fluctuations,” in *Criticality in QCD and the Hadron Resonance Gas*. 1, 2021. [arXiv:2101.02254 \[hep-lat\]](#).
- [29] M. E. Fisher, “Critical point phenomena - the role of series expansions,” *Rocky Mountain Journal of Mathematics* **4** no. 2, (1974) 181.
- [30] J. G. Darboux *J. Math. Pures Appl.* **4**, 377 (1878) .
- [31] G. Baker and P. Graves-Morris, *Padé Approximants*. Cambridge University Press.
- [32] C. Bender and S. Orszag, *Advanced Mathematical Methods for Scientists and Engineers*. Springer, New York.
- [33] H. Stahl, “The convergence of padé approximants to functions with branch points,” *J. Approx. Theor.* **91** (1997) 139–204 .
- [34] A. I. Aptekarev, V. I. Buslaev, A. Martinez-Finkelshtein, and S. Suetin, “Padé approximants, continued fractions, and orthogonal polynomials,” *Russian Math. Surveys* **66:6** (2011) 1049–1131.
- [35] J. Zinn-Justin, “Quantum field theory and critical phenomena,” *Int. Ser. Monogr. Phys.* **113** (2002) 1–1054.
- [36] E. Caliceti, M. Meyer-Hermann, P. Ribeca, A. Surzhykov, and U. D. Jentschura, “From useful algorithms for slowly convergent series to physical predictions based on divergent perturbative expansions,” *Phys. Rept.* **446** (2007) 1–96, [arXiv:0707.1596 \[physics.comp-ph\]](#).
- [37] I. Caprini, J. Fischer, G. Abbas, and B. Ananthanarayan, “Perturbative Expansions in QCD Improved by Conformal Mappings of the Borel Plane,” [arXiv:1711.04445 \[hep-ph\]](#).
- [38] Z. Nehari, *Conformal Mapping*. 1952.

- [39] H. Kober, *Dictionary of Conformal Representations*. Dover, 1957.
- [40] R. Rossi, T. Ohgoe, K. Van Houcke, and F. Werner, “Resummation of diagrammatic series with zero convergence radius for strongly correlated fermions,” *Phys. Rev. Lett.* **121** no. 13, (2018) 130405, [arXiv:1802.07717](https://arxiv.org/abs/1802.07717) [cond-mat.quant-gas].
- [41] M. Serone, G. Spada, and G. Villadoro, “ $\lambda\phi_2^4$ theory — Part II. the broken phase beyond NNNN(NNN)LO,” *JHEP* **05** (2019) 047, [arXiv:1901.05023](https://arxiv.org/abs/1901.05023) [hep-th].
- [42] C. Bertrand, S. Florens, O. Parcollet, and X. Waintal, “Reconstructing Nonequilibrium Regimes of Quantum Many-Body Systems from the Analytical Structure of Perturbative Expansions,” *Phys. Rev. X* **9** (2019) 041008, [1903.11646](https://arxiv.org/abs/1903.11646).
- [43] O. Costin and G. V. Dunne, “Physical Resurgent Extrapolation,” *Phys. Lett. B* **808** (2020) 135627, [arXiv:2003.07451](https://arxiv.org/abs/2003.07451) [hep-th].
- [44] A. Erdélyi, ed., *Higher Transcendental Functions, The Bateman Manuscript Project, vol 1*. Krieger, New York. <https://authors.library.caltech.edu/43491/>.
- [45] W. Abikoff, “The uniformization theorem,” *Am. Math. Mon.* **88** (1981) 574-592 .
- [46] O. Costin, “Interactive realization of uniformization map trajectories,” 2021. <https://people.math.osu.edu/costin.9/classes.html>.
- [47] “NIST Digital Library of Mathematical Functions.” [Http://dlmf.nist.gov/](http://dlmf.nist.gov/), release 1.1.3 of 2021-09-15. <http://dlmf.nist.gov/>. F. W. J. Olver, A. B. Olde Daalhuis, D. W. Lozier, B. I. Schneider, R. F. Boisvert, C. W. Clark, B. R. Miller, B. V. Saunders, H. S. Cohl, and M. A. McClain, eds.
- [48] W. Florkowski, M. P. Heller, and M. Spalinski, “New theories of relativistic hydrodynamics in the LHC era,” *Rept. Prog. Phys.* **81** no. 4, (2018) 046001, [arXiv:1707.02282](https://arxiv.org/abs/1707.02282) [hep-ph].
- [49] I. Aniceto, B. Meiring, J. Jankowski, and M. Spaliński, “The large proper-time expansion of Yang-Mills plasma as a resurgent transseries,” *JHEP* **02** (2019) 073, [arXiv:1810.07130](https://arxiv.org/abs/1810.07130) [hep-th].
- [50] R. Guida and J. Zinn-Justin, “Critical exponents of the N vector model,” *J. Phys. A* **31** (1998) 8103–8121, [arXiv:cond-mat/9803240](https://arxiv.org/abs/cond-mat/9803240).
- [51] D. J. Wallace and R. K. P. Zia, “Parametric models and the ising equation of state at order epsilon3,” *Journal of Physics C: Solid State Physics* **7** no. 19, (Oct, 1974) 3480–3490. <https://doi.org/10.1088/0022-3719/7/19/008>.